



Deposited via The University of Sheffield.

White Rose Research Online URL for this paper:

<https://eprints.whiterose.ac.uk/id/eprint/100034/>

Version: Accepted Version

Article:

Mobasher, N., Bernal, S.A., Hussain, O.H. et al. (2014) Characterisation of Ba(OH)(2)-Na₂SO₄-blast furnace slag cement-like composites for the immobilisation of sulfate bearing nuclear wastes. Cement and Concrete Research, 66. pp. 64-74. ISSN: 0008-8846

<https://doi.org/10.1016/j.cemconres.2014.07.006>

Reuse

This article is distributed under the terms of the Creative Commons Attribution-NonCommercial-NoDerivs (CC BY-NC-ND) licence. This licence only allows you to download this work and share it with others as long as you credit the authors, but you can't change the article in any way or use it commercially. More information and the full terms of the licence here: <https://creativecommons.org/licenses/>

Takedown

If you consider content in White Rose Research Online to be in breach of UK law, please notify us by emailing eprints@whiterose.ac.uk including the URL of the record and the reason for the withdrawal request.

1 **Characterisation of Ba(OH)₂-Na₂SO₄-blast furnace slag cement-like** 2 **composites for the immobilisation of sulphate bearing nuclear wastes**

3
4
5 Neda Mobasher¹, Susan A. Bernal¹, Oday H. Hussain¹, David C. Apperley², Hajime
6 Kinoshita¹, John L. Provis^{1*}

7
8 *¹Immobilisation Science Laboratory, Department of Materials Science & Engineering,*
9 *The University of Sheffield, Sheffield S1 3JD, United Kingdom*

10 *²Solid-State NMR Group, Department of Chemistry, Durham University, Durham DH1 3LE,*
11 *United Kingdom*

12
13 * To whom correspondence should be addressed. Email j.provis@sheffield.ac.uk,
14 phone +44 114 222 5490, fax +44 114 222 5493

15 16 **Abstract**

17
18 Soluble sulphate ions in nuclear waste can have detrimental effects on cementitious
19 wasteforms and disposal facilities based on Portland cement. As an alternative, Ba(OH)₂-
20 Na₂SO₄-blast furnace slag composites are studied for immobilisation of sulphate-bearing
21 nuclear wastes. Calcium aluminosilicate hydrate (C-A-S-H) with some barium substitution is
22 the main binder phase, with barium also present in the low solubility salts BaSO₄ and BaCO₃,
23 along with Ba-substituted calcium sulphoaluminate hydrates, and a hydrotalcite-type layered
24 double hydroxide. This reaction product assemblage indicates that Ba(OH)₂ and Na₂SO₄ act
25 as alkaline activators and control the reaction of the slag in addition to forming insoluble
26 BaSO₄, and this restricts sulphate availability for further reaction as long as sufficient
27 Ba(OH)₂ is added. An increased content of Ba(OH)₂ promotes a higher degree of reaction,
28 and the formation of a highly cross-linked C-A-S-H gel. These Ba(OH)₂-Na₂SO₄-blast
29 furnace slag composite binders could be effective in the immobilisation of sulphate-bearing
30 nuclear wastes.

31
32 **Keywords:** alkali-activated cements; granulated blast furnace slag; sulphate-bearing nuclear
33 waste; barium; microstructure

34

35 **1. Introduction**

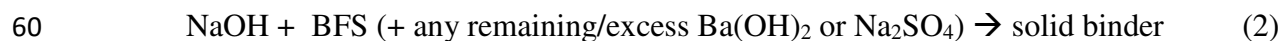
36

37 The immobilisation of sulphate bearing radioactive waste generated in the nuclear industry is
38 difficult to achieve effectively via vitrification or traditional cementing processes, which are
39 the most common methodologies used worldwide for the immobilisation of low and
40 intermediate level nuclear wastes. The presence of soluble sulphate during vitrification causes
41 phase separation in borosilicate glass [1], and in the case of cement-based materials it can
42 promote microstructural changes in the long term [2-4], such as expansion and cracking
43 through the process of internal sulphate attack, which may result in the release of
44 radionuclides into the environment. If sulphate-containing nuclear waste is not treated and
45 encapsulated effectively, it can also interact with any Portland cement-based backfill or
46 structural concrete used in a repository, potentially causing decay of the repository structure
47 through sulphate attack processes. Calcium aluminate or sulphotoaluminate cement-based
48 materials can sometimes accommodate much higher sulphate contents without undergoing
49 degradation processes, but also offer handling and processing challenges in this application.

50

51 Asano et al. [5] proposed an alternative method for the solidification/stabilisation of sulphate-
52 rich aqueous low level wastes using Ba(OH)₂ and slag, via a two-step process in which a
53 cement-like solid can be formed. In their method, Na₂SO₄ (simulated waste) solution was
54 mixed with Ba(OH)₂ in the first step, stabilising the sulphate ions through the precipitation of
55 the highly insoluble phase BaSO₄ and releasing NaOH (reaction 1), followed by a second step
56 of blending the alkaline BaSO₄-containing slurry (produced in the first step) with blast
57 furnace slag (BFS) to produce a cement-like solid (reaction 2).

58



61

62 Recently, Mobasher et al. [6] published a proof-of-concept of a one-step process to produce
63 solid wasteforms with comparable chemistry to those assessed by Asano et al. [5] for
64 immobilisation of sulphate bearing aqueous waste, formulating Ba(OH)₂-Na₂SO₄-BFS
65 composites. In this one-step process, reactions (1) and (2) take place simultaneously. The
66 reaction scheme developed effectively results in an alkali-activation process, with the
67 Ba(OH)₂ and Na₂SO₄, as well as NaOH generated in situ, interacting with the slag to form a

68 hardened binder. A single-step approach has advantages from an operational point of view,
69 compared with that proposed by Asano et al. [5], as less manipulation of the aqueous waste is
70 favourable for adequate disposal. Cement-like systems of this type would be beneficial not
71 only because of the formation of very low-solubility BaSO₄ [7], but also because BaSO₄ can
72 enhance the radiation shielding properties of a wasteform or concrete due to the high atomic
73 number of Ba [8]. Additionally, the presence of BaSO₄ in these binders can be useful for co-
74 precipitation of radionuclides such as ⁹⁰Sr that can be present in the aqueous waste [9].

75

76 When BFS reacts with a source of alkalis to form a hardened binder, the main reaction
77 product and strength-giving phase is a calcium-silicate-hydrate (C-S-H) type phase with a
78 low Ca/Si ratio and a significant degree of aluminium substitution, termed C-A-S-H [10, 11].
79 The structure and composition of the C-A-S-H and secondary reaction products forming in
80 alkali-activated slag binders are strongly dependent on the nature of the activator selected
81 [12-15], the activation conditions adopted [16], and the chemical composition of the slag
82 used [17-19]. In the case of silicate- and hydroxide-activated slags, for instance, layered
83 double hydroxide compounds have been observed [20-23]. When Na₂SO₄ is used as the sole
84 activator, the main secondary product is ettringite [24, 25], because of the increased content
85 of sulphate available in the system.

86

87 It is, therefore, important to understand the activation reaction of the slag in these
88 cementitious wasteforms, as the development of the main binding phase can have a
89 significant influence on the chemistry and microstructure of the system, which in return has a
90 direct impact on radionuclide binding and the permeability of gases and liquids through the
91 solid, and thus wasteform performance. This is of particular interest for the Ba(OH)₂-Na₂SO₄-
92 BFS composite system, as this system has different constituents which can potentially act as
93 an activator i.e., Ba(OH)₂, Na₂SO₄ and NaOH. The published literature does not contain
94 detailed chemical or microstructural characterisation of Ba(OH)₂-activated slags, and
95 therefore the role of Ba(OH)₂ in the activation and structural development of these materials
96 is still unknown.

97

98 In this study Ba(OH)₂-Na₂SO₄-BFS composite pastes, formulated with different Ba(OH)₂ to
99 Na₂SO₄ ratios, are evaluated via X-ray diffraction (XRD), nuclear magnetic resonance
100 (NMR), and scanning electron microscopy (SEM) coupled with energy dispersive X-ray
101 (EDX) spectroscopy. To determine the individual roles of Ba(OH)₂ and Na₂SO₄ in the alkali-

102 activation reaction of the slag, samples activated with each compound individually are also
103 evaluated, in addition to samples activated with NaOH to provide comparative information.

104
105
106

107 2. Experimental programme

108 2.1. Materials

109

110 A blast furnace slag (BFS) from Redcar steelworks with a specific surface of 286 m²/kg was
111 used as the main solid precursor, and its chemical composition is presented in Table 1.
112 Barium hydroxide octahydrate (Ba(OH)₂·8H₂O, 97% purity) and sodium sulphate (Na₂SO₄,
113 99% purity) from Alfa Aesar, and sodium hydroxide (NaOH, general purpose grade) from
114 Fisher Scientific, were used to produce the composites.

115

116 **Table 1.** Composition of blast furnace slag (BFS), from X-ray fluorescence analysis. LOI is
117 loss on ignition at 1000°C

Component as oxides	CaO	SiO ₂	Al ₂ O ₃	Fe ₂ O ₃	MgO	K ₂ O	Na ₂ O	SO ₃	others	LOI
Weight %	38.8	35.8	13.4	0.9	7.6	0.4	0.3	0.7	1.2	0.9

118

119

120 2.2. Sample preparation and tests conducted

121

122 A simulated aqueous sulphate-bearing waste (10 wt.% Na₂SO₄) was prepared by dissolving
123 solid anhydrous Na₂SO₄ in distilled water at 40°C, and then mixed with a homogeneous
124 blend of unreacted BFS and powdered Ba(OH)₂·8H₂O in a sealed plastic container. The
125 samples were manually shaken for 2 to 5 minutes at room temperature, and then mixed for 5
126 more minutes using a Whirl Mixer. Detailed formulations of the specimens produced are
127 given in Table 2.

128

129

130

131

132 **Table 2.** Formulations of Na₂SO₄-Ba(OH)₂-BFS composites and alkali-activated BFS. The
 133 water/binder (w/b) ratio column includes water incorporated as part of the hydrated barium
 134 hydroxide.

Sample ID	Ba ²⁺ :SO ₄ ²⁻		BFS (g)	H ₂ O (g)	Na ₂ SO ₄ (g)	Ba(OH) ₂ ·8H ₂ O (g)	NaOH (g)
	molar ratio	w/b					
BFS + Na ₂ SO ₄		0.34	100	34	39	0	0
BFS + Ba(OH) ₂		0.37	100	37	0	11.23	0
BFS + NaOH		0.34	100	34	0	0	2.2
M1.0	1.0 : 1.0	0.36	100	36	39	8.64	0
M1.3	1.3 : 1.0	0.37	100	37	39	11.23	0

135
 136 The same procedure was used to prepare the reference samples for the assessment of the role
 137 of Ba(OH)₂, Na₂SO₄ and NaOH in the activation procedure. The contents of Ba(OH)₂ and
 138 Na₂SO₄ in the reference specimens were based on the formulation of M1.3, but using each of
 139 the activator components individually. The amount of NaOH used in that reference sample
 140 was calculated to match the quantity which would be generated by a stoichiometric chemical
 141 reaction between the amounts of Na₂SO₄ and Ba(OH)₂ present in sample M1.3 to produce
 142 BaSO₄ and NaOH.

143
 144 Specimens were cured for 180 days at room temperature under sealed conditions, then
 145 demoulded, crushed and immersed in acetone to arrest the reaction process. After several
 146 days, the samples were removed from the acetone, dried to remove the solvent, and
 147 desiccated under vacuum. The dried samples were kept in sealed containers prior to analysis
 148 to avoid carbonation.

149
 150 Characterisation of the pastes was conducted by:

- 151 • X-ray diffraction (XRD), using a Siemens D5000 X-ray diffractometer with
 152 monochromatic Cu K α radiation, operated at a step size of 0.02° and a scanning speed of
 153 0.5°/min between 5° and 55° 2 θ . Specimens were ground using an agate mortar and
 154 pestle, and sieved to < 63 μ m prior to the measurement.
- 155 • Thermogravimetric analysis (TGA), using a Perkin Elmer Pyris 1 TGA. Approximately
 156 40 mg of sample was placed in an alumina crucible. The samples were heated under a
 157 flowing nitrogen atmosphere at a heating rate of 10°C/min from room temperature up to
 158 1000°C.

- 159 • Solid-state ^{29}Si MAS NMR spectra were collected at 59.56 MHz on a Varian Unity
160 Inova 300 (7.05 T) spectrometer using a probe for 7.5 mm o.d. zirconia rotors and a
161 spinning speed of 5 kHz. The ^{29}Si MAS experiments employed a 90° pulse of duration 5
162 μs , a relaxation delay of 5 s and 14000 scans. Solid-state ^{27}Al MAS NMR spectra were
163 acquired at 104.198 MHz, using a Varian VNMRs 400 (9.4T) spectrometer and a probe
164 for 4 mm o.d. zirconia rotors and a spinning speed of 14 kHz with a pulse width of 1 μs
165 (approximately 25°), a relaxation delay of 0.2 s, and a minimum of 7000 scans. ^{23}Na
166 MAS NMR spectra were collected on the VNMRs spectrometer at 105.78 MHz using a
167 probe for 4 mm o.d. zirconia rotors and a spinning speed of 10 kHz with a pulse width of
168 1 μs (approximately 25°), a relaxation delay of 1 s, and a minimum of 2000 scans. ^{29}Si ,
169 ^{27}Al , ^{23}Na chemical shifts are referenced to external samples of tetramethylsilane (TMS),
170 a 1.0 M aqueous solution of $\text{Al}(\text{NO}_3)_3$, and a 0.1M aqueous solution of NaCl,
171 respectively.
- 172 • Scanning electron microscopy (SEM), using a JEOL electron microscope, JSM 6400,
173 with a backscattered electron detector and an accelerating voltage of 20 keV. Epoxy resin
174 (EpoxiCure TM) was poured over the samples, which were then held under vacuum to
175 minimise entrapped air. The samples were removed from the vacuum after
176 approximately 15 minutes and left for 24 hours to harden before sanding manually with
177 grinding papers of 400 and 1200 grit SiC. Samples were then polished with 1 μm and
178 0.25 μm diamond pastes and polishing cloths. The samples were finally coated with
179 carbon using an Edwards ‘speedivac’ carbon coating unit and silver dagged to make
180 them electrically conductive before analysis.

181

182 **3. Results and discussion**

183

184 **3.1. X-ray diffraction**

185

186 The X-ray diffractograms of the reference samples of BFS activated with Na_2SO_4 , NaOH and
187 $\text{Ba}(\text{OH})_2$ are compared with that of the unreacted slag in Figure 1. The unreacted slag is
188 predominantly amorphous, and contains minor traces of the melilite type phase åkermanite
189 ($\text{Ca}_2\text{MgSi}_2\text{O}_7$, powder diffraction file, PDF, #076-0841), and calcite (CaCO_3 , PDF #005-
190 0586) due to slight weathering. Upon activation with Na_2SO_4 , formation of ettringite (PDF #
191 041-1451) is identified, in agreement with what has previously been reported for similar

192 systems [24, 25]. A small peak at $11.3^\circ 2\theta$ is also observed in these samples, and is assigned
193 to a layered double hydroxide in the hydrotalcite group ($\text{Mg}_6\text{Al}_2(\text{CO}_3)(\text{OH})_{16}\cdot 4\text{H}_2\text{O}$, PDF #
194 089-0460). In alkali-activated slags with moderate to high MgO contents, such layered
195 double hydroxides are usually produced as a secondary reaction product [17, 19]. Disordered
196 C-S-H type gel products are also identified in all samples by a very broad peak centred just
197 below $30^\circ 2\theta$.

198

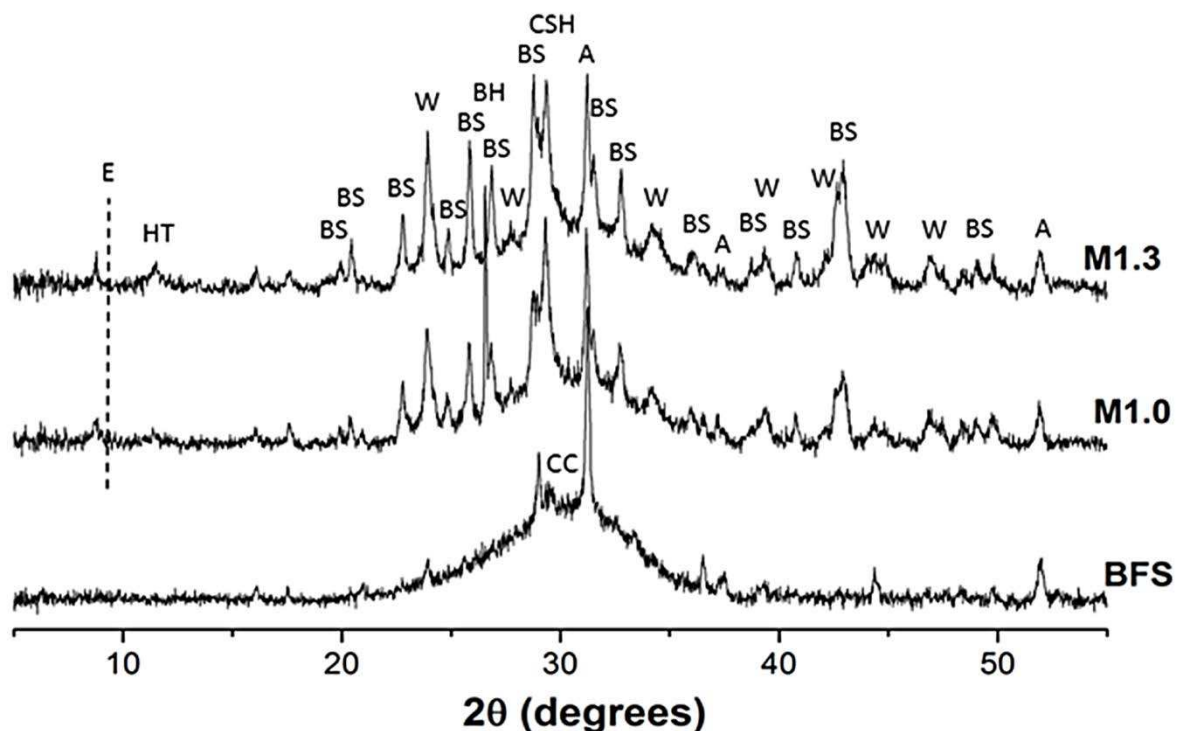
199 In the NaOH-activated slag, ettringite is not forming, consistent with the absence of sulphates
200 in the system, and instead hemicarbonate-AFm ($(\text{CaO})_3\cdot \text{Al}_2\text{O}_3\cdot 0.5\text{CaCO}_3\cdot 12\text{H}_2\text{O}$, PDF #
201 036-0129) is observed along with hydrotalcite. Identification of AFm type phases in NaOH-
202 activated slag binders is difficult to achieve via X-ray diffraction [20, 22, 26]; however,
203 formation of this type of phase has been suggested through analysis of NaOH-activated slag
204 binders by NMR spectroscopy [23, 27], potentially as a crystallographically disordered phase
205 intermixed with the C-A-S-H products [28].

206

207 In the $\text{Ba}(\text{OH})_2$ activated slag sample, a reflection consistent with the position of the main
208 hydrotalcite peak just above $10^\circ 2\theta$ was observed, with a slight shift towards lower 2θ
209 compared to the hydrotalcite reference pattern. This indicates an increased d -spacing in this
210 phase, which may correspond to some Ba^{2+} incorporation as a larger cation substituting for
211 the smaller Mg^{2+} . Although this has not previously been noted as a possibility in the literature
212 for such phases, and the cationic radii are very different, Glasser [29] has reported
213 substitution of Ca^{2+} by Ba^{2+} in crystalline cement phases. In addition, it has been observed
214 that AFm phases, a type of layered double hydroxides are highly susceptible to cation
215 exchange at room temperature, with compositions very sensitive to their local chemical
216 environment [30]., Therefore, Ba substitution in layered double hydroxides such as
217 hydrotalcite-like and AFm type phases could be plausible in the $\text{Ba}(\text{OH})_2$ -activated slag
218 binder.

219

220



239
240 **Figure 2.** X-ray diffractograms of unreacted slag and $\text{Na}_2\text{SO}_4\text{-Ba(OH)}_2\text{-BFS}$ composites as a
241 function of the Ba^{2+} to SO_4^{2-} molar ratio. Peaks marked are BaSO_4 (BS), åkermanite (A),
242 calcite (CC), witherite (W), ettringite (E), hydrotalcite (HT) and C-A-S-H (CSH). The dashed
243 line indicates the position of the main (100) peak of ettringite.

244
245 In these composites, independent of the Ba(OH)_2 content, the formation of a compound with
246 a peak at $8.50^\circ 2\theta$ is observed (Figure 2). As the peak position is slightly shifted to lower 2θ
247 when compared with the main reflection peak of ettringite ($9.0^\circ 2\theta$), it is likely that in
248 presence of Ba(OH)_2 , formation of a Ba-containing AFt type phase takes place. The
249 substitution of Ba^{2+} in the Ca^{2+} sites in ettringite structure has previously been reported [29,
250 31], and Ba-bearing ettringite has a larger d -spacing than pure ettringite [32], shifting the
251 peak to lower angle as observed in these samples. Utton et al. [33] identified, in a 1:9
252 Portland cement/BFS system containing BaCO_3 , that the formation of ettringite and
253 precipitation of BaSO_4 occur simultaneously, competing for the sulphate ions in the solution.
254 After extended times of curing in those systems, ettringite decomposed to form calcium
255 monocarboaluminate (AFm), calcite and BaSO_4 , by reacting with the free Ba^{2+} ions.
256 Considering that the compounds identified as being stable by Utton et al. [33] are similar to
257 those which form in the $\text{Ba(OH)}_2\text{-Na}_2\text{SO}_4\text{-slag}$ composites here, significant changes in the
258 phase assemblage of the composites are unlikely to occur at advanced times of curing.

259

260 The results obtained here reveal that in the composites assessed in this study, as formation of
261 ettringite takes place as a consequence of the Na_2SO_4 -activation of slag, not all of the
262 sulphate is directly consumed according to equation (1) by BaSO_4 precipitation. Na_2SO_4 will
263 continue promoting the formation of ettringite in the system when its amount exceeds the
264 capacity of $\text{Ba}(\text{OH})_2$ to immediately form BaSO_4 . This observation differs from the trends
265 identified in studies evaluating the effects of $\text{Ba}(\text{OH})_2$ or BaCO_3 on the structures of synthetic
266 ettringite and thaumasite [34-36], where the formation of ettringite was suppressed or ettringite
267 is completely decomposed. In these studies, a large quantity of $\text{Ba}(\text{OH})_2$ was used, suggesting
268 that the content of $\text{Ba}(\text{OH})_2$ would need to be increased in the composite systems to hinder
269 the formation of ettringite.

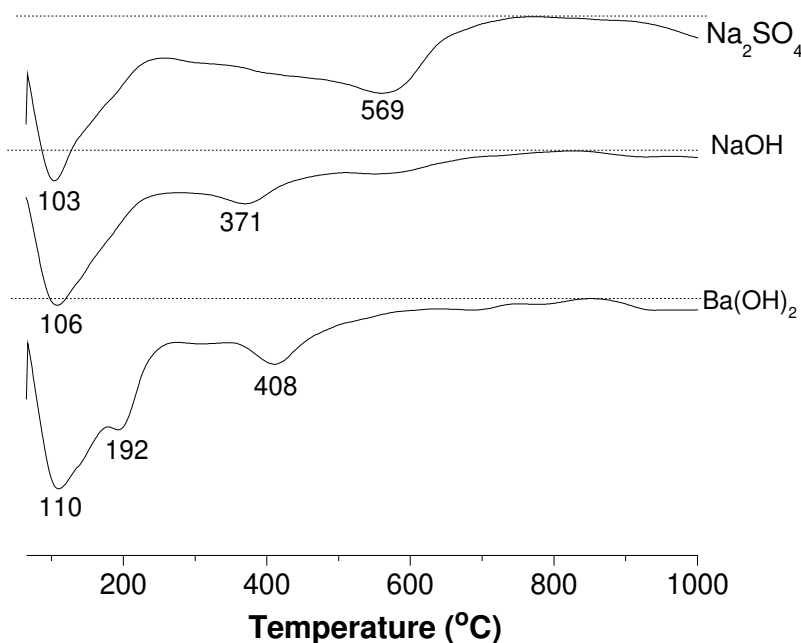
270

271

272 3.2 Thermogravimetry

273

274 Figure 3 shows the differential thermograms (DTG) of Na_2SO_4 -activated BFS, NaOH -
275 activated BFS and $\text{Ba}(\text{OH})_2$ -activated BFS pastes. The total loss of weight up to 1000°C for
276 Na_2SO_4 -activated BFS is 13.9%, for NaOH -activated BFS 12.06%, and for $\text{Ba}(\text{OH})_2$ -
277 activated BFS 16.4%.



278

279 **Figure 3.** Differential thermograms (mass loss downwards) of alkali-activated BFS with
280 different alkaline activators. Dashed lines show the baseline for each data set.

281 In the Na₂SO₄-activated BFS, a high intensity peak between 70°C and 200°C is observed,
282 which is attributed to the release of evaporable water in the system, and the start of the
283 dehydration of ettringite [37], as was identified through XRD (Figure 1). The progressive
284 weight loss between 200°C and 400°C is assigned to the decomposition of the C-A-S-H [38]
285 also identified through XRD. The low intensity shoulder around 569°C is attributed to the
286 decomposition of calcite [39]. In NaOH-activated and Ba(OH)₂-activated samples, the weight
287 loss around 200°C and 400°C is assigned to the hydrotalcite like-phase and the decomposition
288 of AFm type compounds present in the sample [40, 41]. The first weight loss peak around
289 192°C in the Ba(OH)₂-activated sample corresponds to the removal of the interlayer water
290 molecules of hydrotalcite, and the second peak around 408°C is assigned to the
291 dehydroxylation of the brucite-like layers [42]. The hydrotalcite peaks are more distinct in the
292 BFS+Ba(OH)₂ sample, consistent with a higher extent of reaction of the slag, and potentially
293 more ordering of the structure of this phase when using Ba(OH)₂ as the alkaline activator.

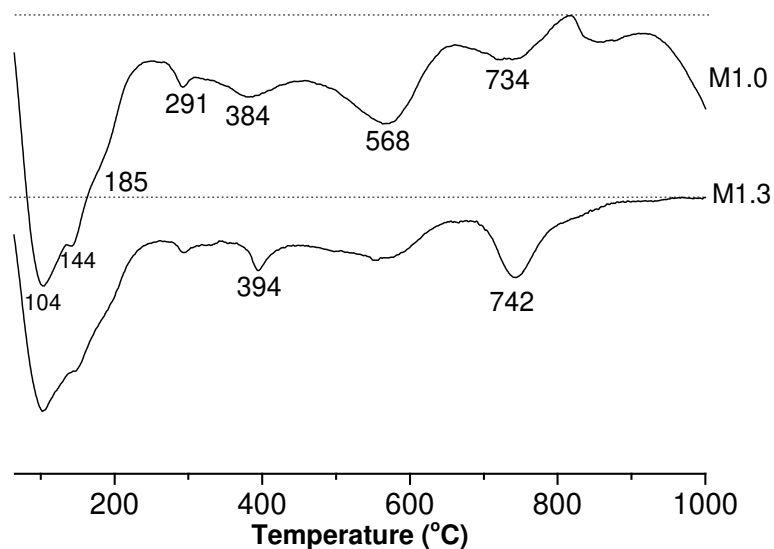
294

295 Figure 4 shows the differential thermograms (DTG) of unreacted slag and Na₂SO₄-Ba(OH)₂-
296 BFS composites with different Ba²⁺:SO₄²⁻ molar ratios. The total weight loss up to 1000°C
297 for M1.0 is 14.58%, and 10.25% for M1.3. The BaSO₄ decomposition temperature is above
298 1000°C [36], and therefore it is not observed in these thermogravimetry data.

299

300 In M1.0 a higher intensity weight loss is observed below 270°C compared with M1.3, which
301 suggests a larger amount of evaporable water in that sample, or potentially the formation of a
302 larger amount of hydration products with water less tightly bonded to the structure than in
303 M1.3. Even though AFm phases were not identified via X-ray diffraction in these samples
304 (Figure 2), it is possible that the minor contributions observed at 144°C and 291°C are
305 associated with decomposition of partially ordered calcium monosulphoaluminate hydrates
306 [41]. Weight losses at 568°C and ~740°C are assigned to the decomposition of the calcium
307 carbonate products present in the composite samples [43]. Decomposition of the hydrotalcite
308 type phase observed in these composites is detected at 185°C and 394°C, and the minor
309 weight loss above 800°C is assigned to decomposition of witherite [36].

310



311
312 **Figure 4.** Differential thermograms (mass loss downwards) for Na₂SO₄-Ba(OH)₂-BFS
313 composites with different Ba²⁺:SO₄²⁻ molar ratios. Dashed lines show the baseline for each
314 data set

315

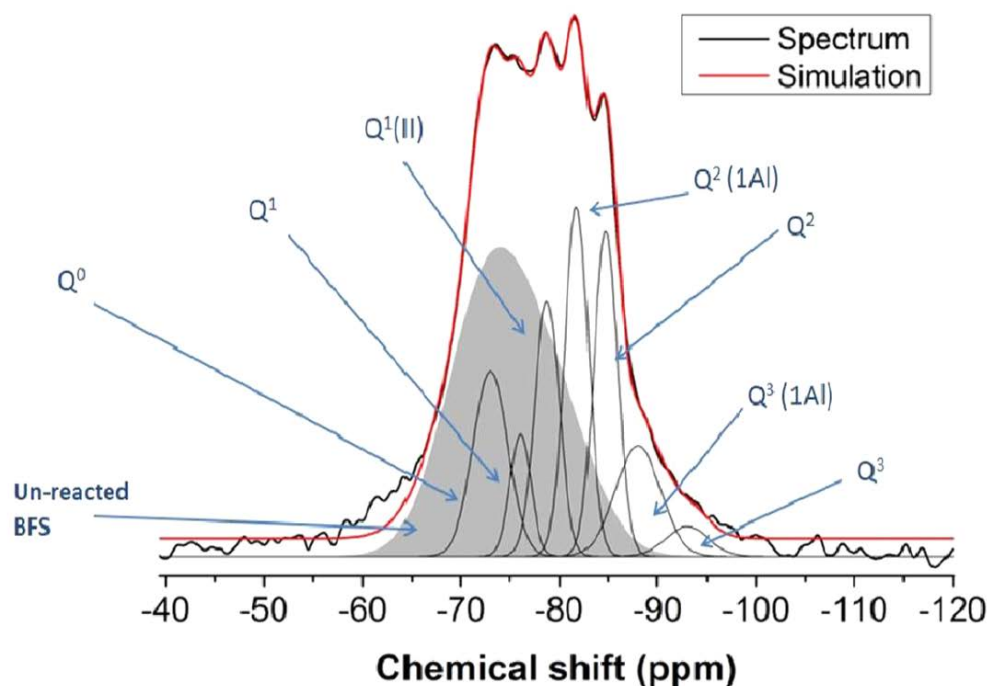
316

317 3.3 Solid-state ²⁹Si MAS NMR spectroscopy

318

319 Solid state ²⁹Si MAS NMR can provide information regarding the fractions of silicon present
320 in various tetrahedral environments in silicates [44]. Deconvolutions of the spectra collected
321 here were carried out according to the procedure described in [43]. An example of a
322 deconvoluted spectrum is shown in Figure 5.

323



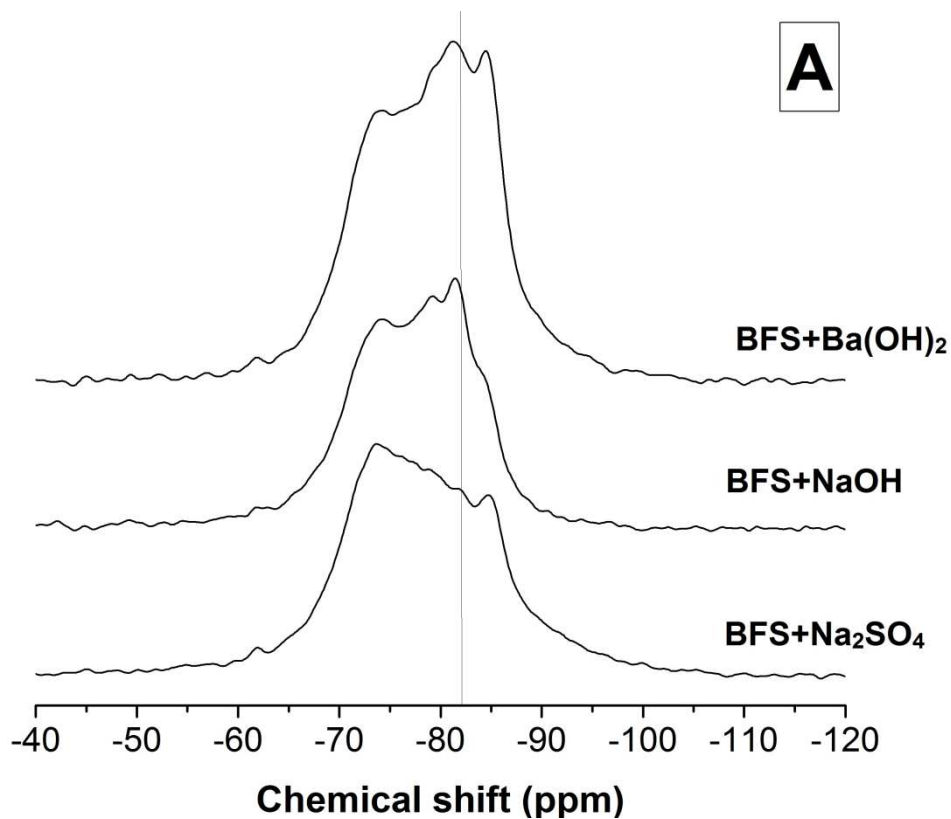
324
325 **Figure 5.** Deconvoluted ^{29}Si MAS NMR spectrum of composite M1.0. The grey area
326 corresponds to the fraction of unreacted slag.

327
328 The resonances identified in the deconvoluted spectra are assigned to connectivity states
329 based on the information available for cements [28, 45], alkali-activated slags [19, 43] and
330 aluminosilicate zeolite systems [44]. It has been proposed that it is possible to determine the
331 degree of reaction of alkali-activated slag binders through the deconvolution of ^{29}Si MAS
332 NMR spectra, as the spectral line shape of the remnant unreacted slag in the activated
333 samples is similar to the line shape of the anhydrous slag [46], and a similar approach was
334 adopted in this study. The lineshape in the downfield region (-60 to -70 ppm) in all reaction
335 product spectra is consistent with this hypothesis of congruent or near-congruent dissolution
336 of the slag, as there is not a notable change in the profile in this region between the spectra of
337 the anhydrous slag and the composite cements.

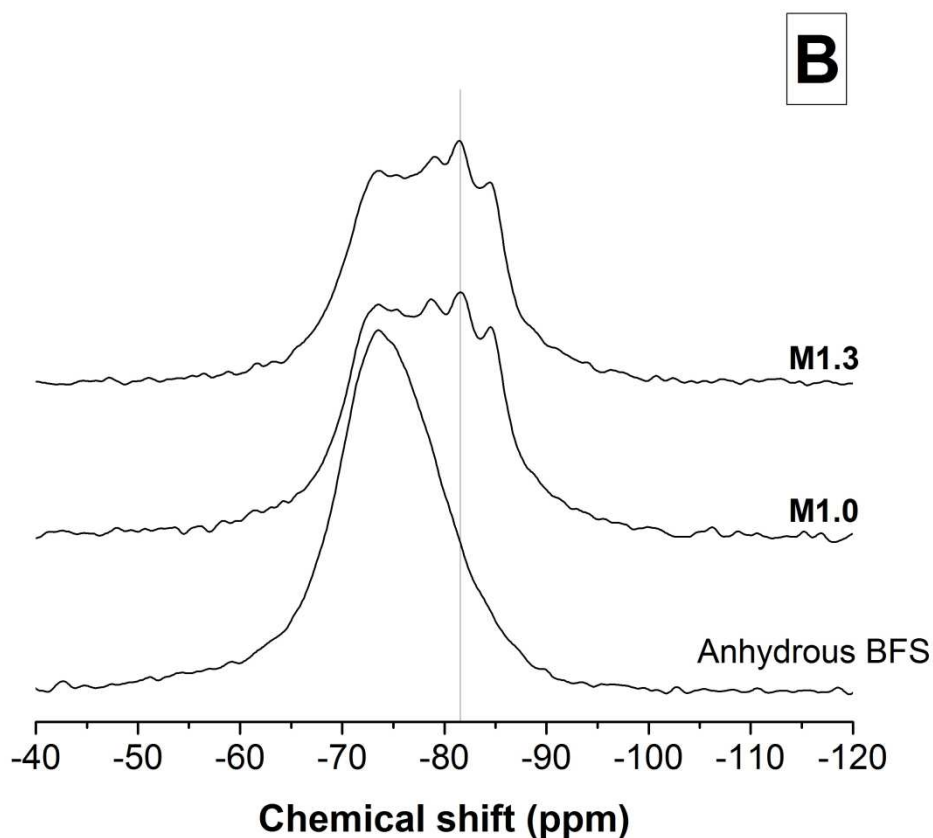
338
339 Figure 6A shows the ^{29}Si MAS NMR spectra of Na_2SO_4 -activated BFS, NaOH -activated BFS
340 and $\text{Ba}(\text{OH})_2$ -activated BFS pastes, while Figure 6B shows those of the unreacted slag, and
341 the M1.0 and M1.3 composites. The unreacted slag has a line shape comparable to the
342 spectrum reported for åkermanite [43], which is identified as the main crystalline phase in the

343 slag used in this study (Figure 2) with a resonance centred at -74 ppm. A reduction of this
344 peak indicates the reaction of the slag in the hydrated samples. In the activated samples
345 resonances between -80 ppm and -90 ppm are identified, consistent with the formation of a
346 C-A-S-H type phase. In particular, resonances between -82 ppm and -85 ppm, corresponding
347 to $Q^2(1Al)$ and Q^2 sites respectively, are assigned to this Al-substituted C-S-H type gel with a
348 tobermorite type structure [28, 47].

349



350



351

352 **Figure 6.** ^{29}Si MAS NMR spectra of (A) Na_2SO_4 -activated BFS, NaOH -activated BFS and
353 $\text{Ba}(\text{OH})_2$ -activated BFS pastes, and (B) unreacted slag, and Na_2SO_4 - $\text{Ba}(\text{OH})_2$ -BFS
354 composites M1.0 and M1.3. Dashed lines indicate the position of $\text{Q}^2(1\text{Al})$ sites.

355

356 Figure 6A shows the reduction of the $\text{Q}^2(1\text{Al})$ site (-82 ppm) in the spectrum of the Na_2SO_4 -
357 activated sample compared to the other activated samples, indicating a reduced degree of Al
358 incorporation in the C-A-S-H product. This could be associated with the fact that most of the
359 Al available in the system is consumed in the formation of ettringite in this formulation
360 (Figure 1).

361

362 In the spectra of the composites M1.0 and M1.3 shown in Figure 6B, the intensity of the
363 broad unreacted slag feature centred at -74 ppm decreases with the increased addition of
364 $\text{Ba}(\text{OH})_2$, showing a higher extent of reaction, as shown in Table 3. The addition of $\text{Ba}(\text{OH})_2$
365 in the composite samples seems to favour the incorporation of Al in the C-A-S-H type gel,
366 associated with the increasing intensity of the $\text{Q}^2(1\text{Al})$ peak, and the identification of $\text{Q}^3(1\text{Al})$
367 sites, as reported in Table 3. The observation of $\text{Q}^3(1\text{Al})$ sites in these materials is an
368 indication of crosslinking taking place in the C-A-S-H phase[48]. Although these pastes
369 contain ettringite, which consumes some of the Al supplied by the slag, the content of

370 hydrotalcite is notably lower than in the Ba(OH)₂-activated and NaOH-activated pastes
 371 (Figure 2), and so the availability of Al appears sufficient for this degree of substitution into
 372 the C-A-S-H. The fate of the Mg is, however, unclear at this stage. These results suggest that
 373 the structure of the C-A-S-H type gel forming in the composite binders is a result of a
 374 combined activation process involving both Na₂SO₄ and Ba(OH)₂, as the hydrate phase
 375 assemblages do not match what would be observed if the slag was solely activated by the
 376 NaOH produced in reaction (1). The C-A-S-H type binders forming in the composite
 377 specimens have a high degree of crosslinking associated with the high fractions of Q² and Q³
 378 species.

379

380 According to the quantification of Si sites presented in Table 3, it is observed from the
 381 remnant unreacted slag fraction that the lowest degree of reaction is achieved in the specimen
 382 activated solely with Na₂SO₄, and the highest degree of reaction when Ba(OH)₂ is used as the
 383 sole activator. These observations are in agreement with the thermogravimetry results, where
 384 the highest weight loss was identified in the Ba(OH)₂-activated specimens among all single-
 385 activator systems analysed. This demonstrates that Ba(OH)₂ can act as an effective activator
 386 for producing alkali-activated materials. Consequently, it is likely that the reaction of the
 387 composites assessed here is not exclusively governed by the formation of NaOH as a
 388 secondary product during the reaction of Ba(OH)₂ and Na₂SO₄ to form BaSO₄ (reaction 1),
 389 but rather that the original Ba(OH)₂ and Na₂SO₄ components are also having a significant
 390 impact. The higher reaction extent observed in M1.3 compared to M1.0 also indicates that the
 391 excess Ba(OH)₂ present in this mix leads to an increased extent of reaction.

392

393 **Table 3.** Quantification of Qⁿ environments identified in the ²⁹Si MAS NMR spectra of the
 394 specimens investigated.

Sample ID	Unreacted slag	Site type in reaction products ^a						
		Q ⁰ -74	Q ^{1(I)} -78	Q ^{1(II)} -80	Q ^{2(IAI)} -82	Q ² -85	Q ^{3(IAI)} -89	Q ^{3(OAI)} -94
M1.0	47	9	4	9	12	11	7	2
M1.3	45	9	5	9	11	13	6	2
Na ₂ SO ₄	53	10	6	3	7	12	7	3
NaOH	49	10	5	11	12	10	3	-

Ba(OH) ₂	39	9	5	9	13	16	7	2
---------------------	----	---	---	---	----	----	---	---

395 ^a Estimated uncertainty in all site percentages is $\pm 2\%$, based on the influence of the signal/noise ratio of the
396 spectra on the de-convolution procedures.

397

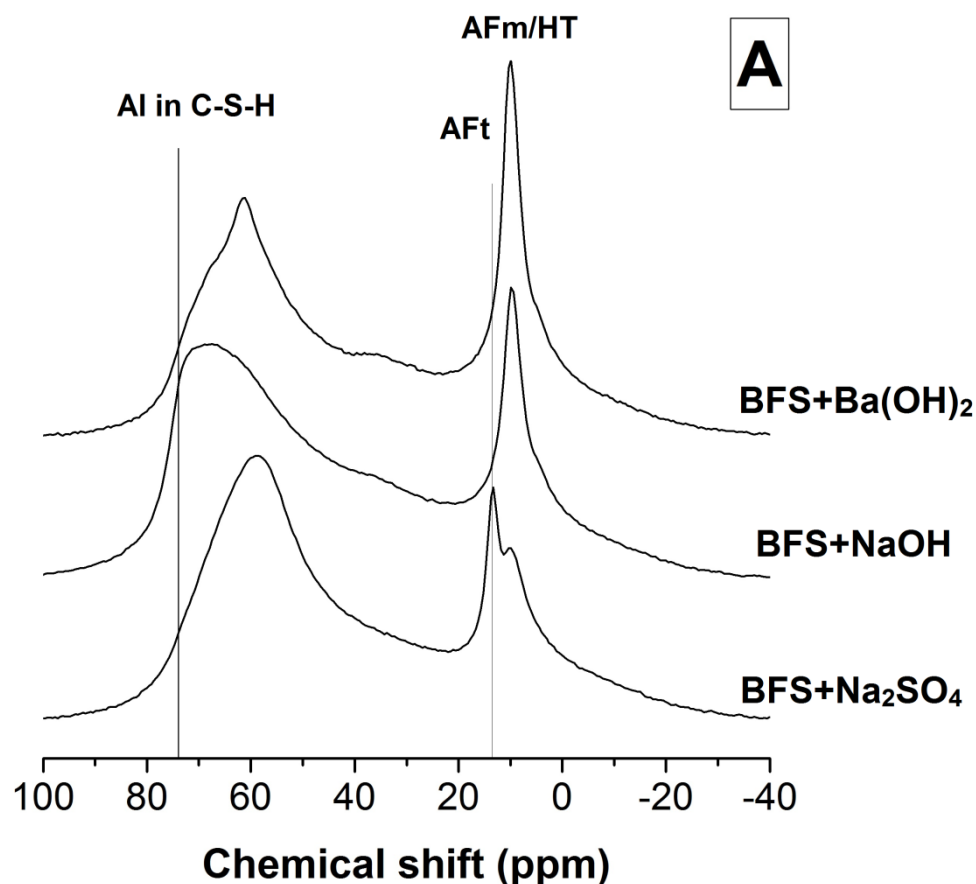
398

399 3.4 Solid-state ²⁷Al MAS NMR spectroscopy

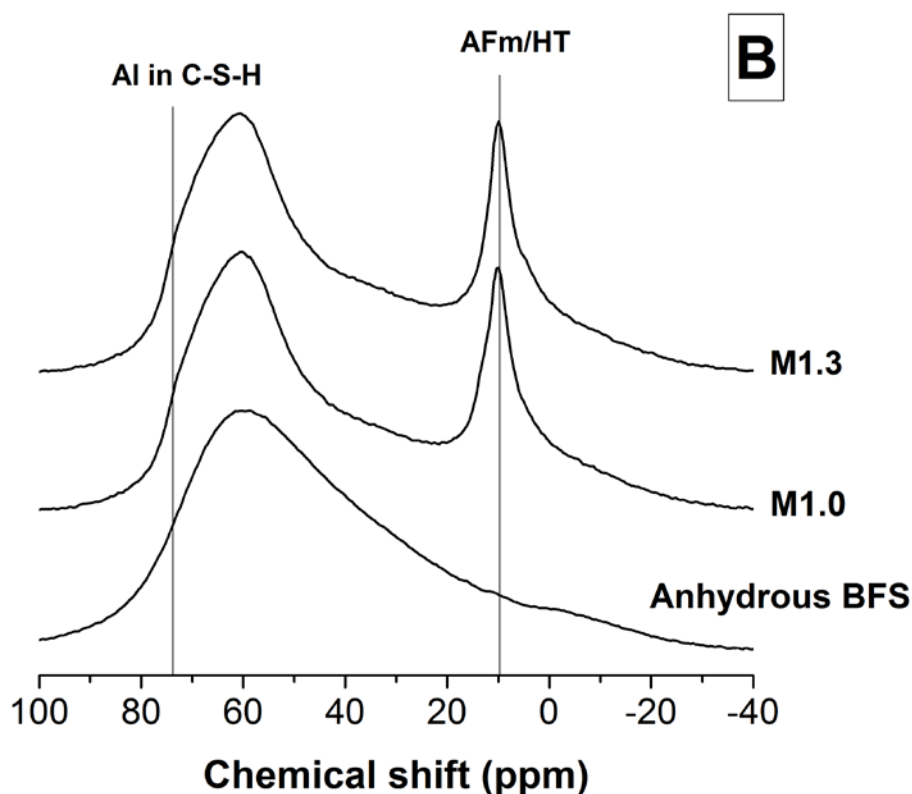
400

401 Figure 7 shows the ²⁷Al MAS NMR spectra of the samples evaluated. The unreacted BFS
402 shows a broad resonance between 40 and 80 ppm, centred around 60 ppm. This region is
403 assigned to tetrahedral Al environments, but cannot be assigned to a well-defined single site
404 type due to structural disorder in the slag. This broad peak is attributed to the glassy phases
405 which comprise the majority of the BFS, consistent with the amorphous hump and low
406 crystalline phase content identified by XRD in the unreacted BFS (Figure 1).

407



408



409

410 **Figure 7.** ^{27}Al MAS NMR spectra of (A) Na_2SO_4 -activated BFS, NaOH-activated BFS and
411 $\text{Ba}(\text{OH})_2$ -activated BFS pastes, and (B) unreacted slag, and $\text{Ba}(\text{OH})_2$ - Na_2SO_4 slag composites
412 M1.0 and M1.3.

413

414 In the Na_2SO_4 -activated BFS sample (Figure 7A), there are two distinguishable peaks in the
415 region associated with octahedrally coordinated Al. The larger peak in this region, at around
416 13 ppm, is assigned to ettringite [49] as identified by XRD (Figure 1). The shoulder at 10
417 ppm is assigned to the hydrotalcite type phase [43] also observed by XRD in this sample,
418 which may also contain minor contributions from AFm type phases as suggested by the DTG
419 analysis, although these are not positively identifiable by XRD. In the NaOH-activated and
420 $\text{Ba}(\text{OH})_2$ -activated pastes, a single peak at 10 ppm is observed in this region of the spectra,
421 and attributed to the layered double hydroxide and AFm type phases, which have very similar
422 ^{27}Al resonance positions.

423

424 The main effect of the activator is identified in the region between 40 ppm and 80 ppm in
425 Figure 7, which is associated with the tetrahedrally coordinated Al. Upon activation a
426 sharpening of the Al(IV) region is identified in all the samples compared with the unreacted
427 BFS; as not all of the slag has reacted, part of the intensity of this band should be assigned to

428 the remnant unreacted BFS. In C-A-S-H products, Al is tetrahedrally coordinated and usually
429 identified at 74 ppm in ^{27}Al MAS NMR spectra [28, 47]. This resonance is observed in
430 NaOH and $\text{Ba}(\text{OH})_2$ activated pastes, consistent with the identification in the ^{29}Si MAS NMR
431 results (Table 3) of high intensity peaks assigned to $\text{Q}^2(1\text{Al})$ sites.

432

433 In the Na_2SO_4 -activated paste, an asymmetric Al(IV) band with a maximum at 60 ppm is
434 instead observed. This resonance is assigned to highly crosslinked Al-rich sites in the C-A-S-
435 H type gel, in agreement with the identification of $\text{Q}^3(1\text{Al})$ sites by ^{29}Si MAS NMR. In the
436 $\text{Ba}(\text{OH})_2$ -activated sample a high intensity peak centred at 61 ppm is identified. Resonances
437 at this specific chemical shift value are consistent with the formation of a poorly ordered
438 AFm type phase (strätlingite) in Al-rich cementitious systems formed under high alkalinity
439 conditions [50]; however, studies of Ba-bearing AFm and/or hydrogarnet phases are very
440 limited, and ^{27}Al MAS NMR spectra of compounds with such chemistry are not available in
441 the open literature to corroborate the assignment of this peak. Considering that Q^3 type sites
442 are observed in the $\text{Ba}(\text{OH})_2$ activated sample in the ^{29}Si MAS NMR spectra, and these sites
443 can be also present in hydrogarnet type phases [51], it is suggested that the formation of a Ba-
444 bearing AFm or hydrogarnet type phase might be occurring. Further investigation to validate
445 this hypothesis is required.

446

447 In the $\text{Ba}(\text{OH})_2$ - Na_2SO_4 -BFS composite samples (Figure 7B) a broad band around 10 ppm
448 with less distinct features than those identified in the NaOH-activated or $\text{Ba}(\text{OH})_2$ -activated
449 slags is observed, and again assigned to the contributions of hydrotalcite type-and ettringite
450 phases, as identified through XRD (Figure 1). The lineshape of the Al(IV) region of the
451 composite spectra does not show significant changes with the addition of different amounts
452 of $\text{Ba}(\text{OH})_2$, consistent with the observation that the C-A-S-H products forming in these
453 systems have very similar structures, as identified via ^{29}Si MAS NMR (Figure 6).

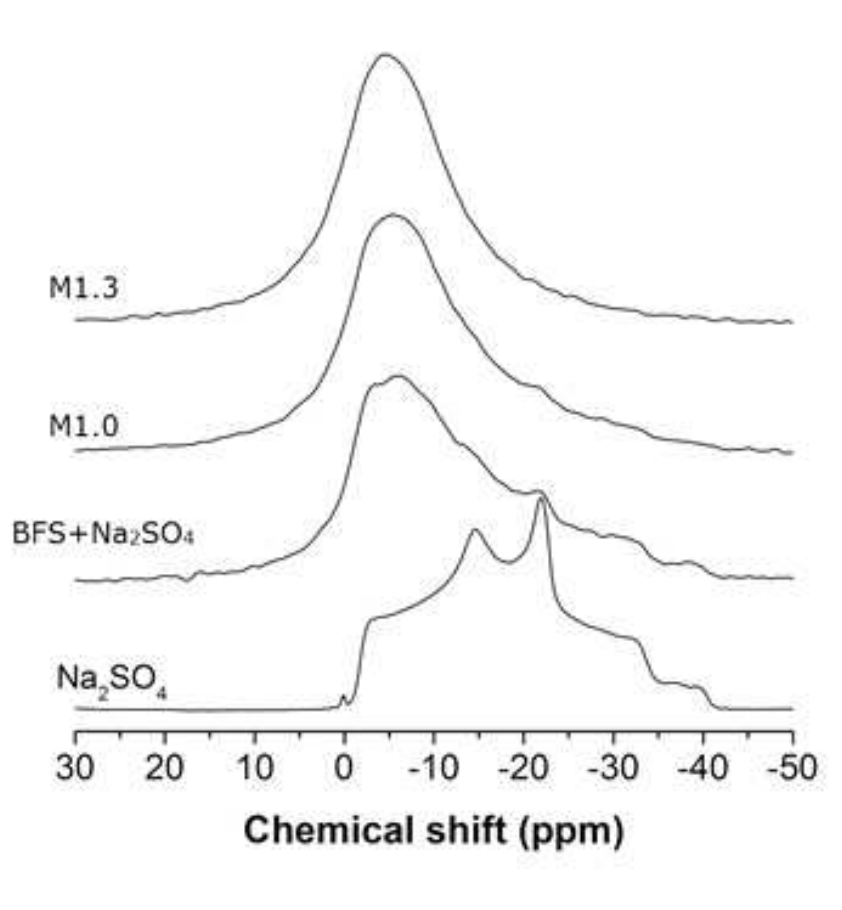
454

455 **3.5 Solid-state ^{23}Na MAS NMR**

456

457 Figure 8 shows the ^{23}Na MAS NMR results for anhydrous Na_2SO_4 , Na_2SO_4 -activated slag
458 and $\text{Ba}(\text{OH})_2$ - Na_2SO_4 slag composite cements. The spectrum collected for anhydrous Na_2SO_4
459 is used here as a reference to identify unreacted Na_2SO_4 in the samples. The line shape of the
460 Na_2SO_4 spectrum is in good agreement with those reported in the literature [52]. It is clear
461 from the spectra of the Na_2SO_4 -activated slag and the composite M1.0 sample that there is

462 some unreacted Na_2SO_4 present in both of these mixes, visible particularly from the sharp
463 resonance at -21 ppm which is seen as a shoulder in the reaction product spectra. This
464 indicates that in the absence of $\text{Ba}(\text{OH})_2$, although some of the sulphate in the waste simulant
465 is chemically bonded through the formation of ettringite, there is an excess of sulphate that is
466 likely to be remaining in the pore solution, and then precipitating as Na_2SO_4 when the
467 samples are dried for analysis. The inclusion of lower contents of $\text{Ba}(\text{OH})_2$ (Figure 8 sample
468 M1.0) reduces the remnant Na_2SO_4 in the sample, due to the formation of BaSO_4 as observed
469 by other analytical techniques; however, there is not complete consumption of Na_2SO_4 . This
470 suggests the need for higher $\text{Ba}(\text{OH})_2$ contents in the system in order to immobilise all of the
471 sulphate bearing waste, as in composite M1.3, where ^{23}Na resonances assigned to remnant
472 Na_2SO_4 are not identified.



473
474 **Figure 8.** ^{23}Na MAS NMR spectra of Na_2SO_4 , Na_2SO_4 -activated BFS, and $\text{Ba}(\text{OH})_2$ - Na_2SO_4 -
475 BFS composite cements M1.0 and M1.3.

476
477 Alkalies play an important role in the properties and microstructure of the products formed
478 during the alkali activation of BFS and aluminosilicate precursors [53]. It is believed that in
479 alkali-activated slag binders, alkalies can be incorporated or physically adsorbed on the

480 surface of the C-A-S-H products through a charge balance mechanism, and also exist free in
481 the pore solution [54, 55]. However, it is likely that the mechanism of uptake of alkalis into
482 the solid phases in alkali-activated materials is strongly dependent on the type of activator
483 used, as this controls the Ca/(Si+Al) ratio of the C-A-S-H type gels, which can vary over the
484 time of curing [20, 26, 56].

485

486 In the alkali-activated composites studied here, a ^{23}Na resonance at around -6 ppm is
487 observed (Figure 8), consistent with the results reported by Bonk et al. [23] for the alkalis in
488 C-A-S-H type gels in alkali-activated slag binders, analysed at a comparable magnetic field.
489 Formation of C-(N)-A-S-H binding phases has been identified in alkali-activated slags via
490 microscopy techniques [18, 57], and it has been proposed that the inclusion of alkalis in the
491 C-A-S-H gel can occur via a charge balancing mechanism where the charge deficit
492 associated with the replacement of a bridging SiO_4 tetrahedron with an AlO_4 unit is balanced
493 by an alkali ion adsorbed/bonded in the interlayer region of the C-S-H phase [58]. It is also
494 clear from the ^{23}Na MAS NMR spectra that the peak at -6 ppm is narrowed in the composite
495 sample M1.3, with a higher amount of $\text{Ba}(\text{OH})_2$, indicating a more ordered gel structure.

496

497 **3.6 Scanning electron microscopy**

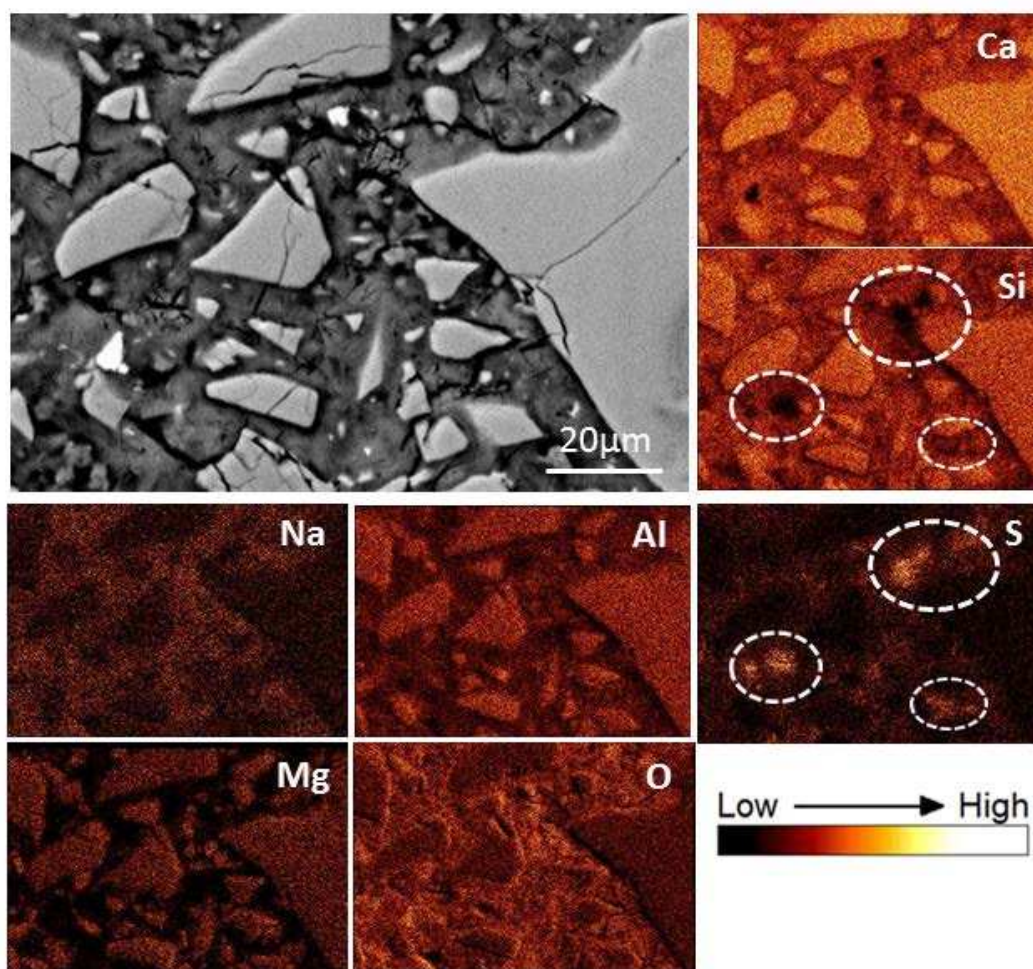
498

499 Figure 9 shows a backscattered electron (BSE) image of the BFS activated with Na_2SO_4 , and
500 elemental distribution in the region of the image. Regions enriched in Ca, Si, Al and Mg
501 correspond to the unreacted slag, whose angular morphology is clear as light grey isolated
502 regions. The binder matrix is mainly composed of Ca, Si and Al, consistent with the
503 formation of a C-A-S-H product, as identified by NMR spectroscopy. An even distribution of
504 Na throughout the binding phase is also observed, consistent with the inclusion of Na in the
505 C-A-S-H type phase as discussed in the analysis of the ^{23}Na MAS NMR results. The regions
506 poor in Si but rich in S (white circles in Figure 9) are identified as ettringite.

507

508

509

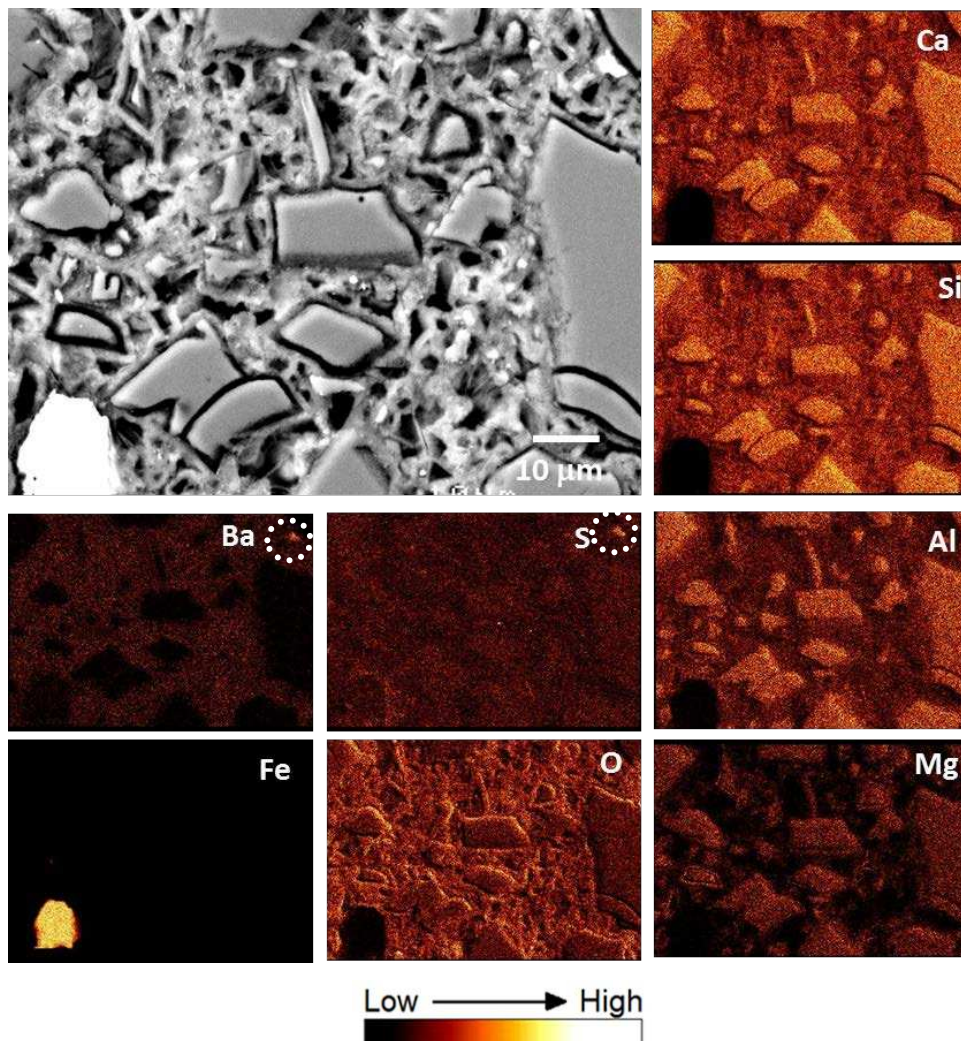


510
511 **Figure 9.** Backscattered electron image and elemental maps of Na_2SO_4 -activated BFS. The
512 elemental maps show the same region as the backscattered electron image.

513
514 Figure 10 shows a BSE image of the BFS sample activated by $\text{Ba}(\text{OH})_2$, and the elemental
515 maps corresponding to this image. This binder shows a highly heterogeneous matrix, with
516 cavities due to the pull-out of unreacted slag particles during sample polishing, as the
517 unreacted slag grains are surrounded by a low-density reaction rim which appears to give
518 little binding to the bulk gel. This is supported by the fact that the cavities (black areas)
519 observed in the BSE have an angular shape consistent with the shape of unreacted slag
520 particles, which would not be the case if those cavities were pores. It is clear from Ba
521 elemental mapping that Ba is incorporated relatively homogeneously throughout the binding
522 matrix, suggesting that the inclusion of some Ba in the C-A-S-H might be occurring in this
523 system. Formation of a C-(Ba)-A-S-H gel has not been observed before, but these results
524 indicate that excess Ba in Ca-rich cementitious systems is not only able to influence sulphate
525 and carbonate rich phases, as has been observed with the inclusion of BaCO_3 [33, 36], but

526 also possibly participate in the C-A-S-H type phase if the concentrations of sulphate and
527 carbonate are low.

528



529

530

531 **Figure 10.** Backscattered electron image and elemental maps of Ba(OH)₂-activated slag. The
532 elemental maps show the same region as the backscattered electron image. Dashed circles in
533 Ba and S maps highlight a BaSO₄ particle forming in this system

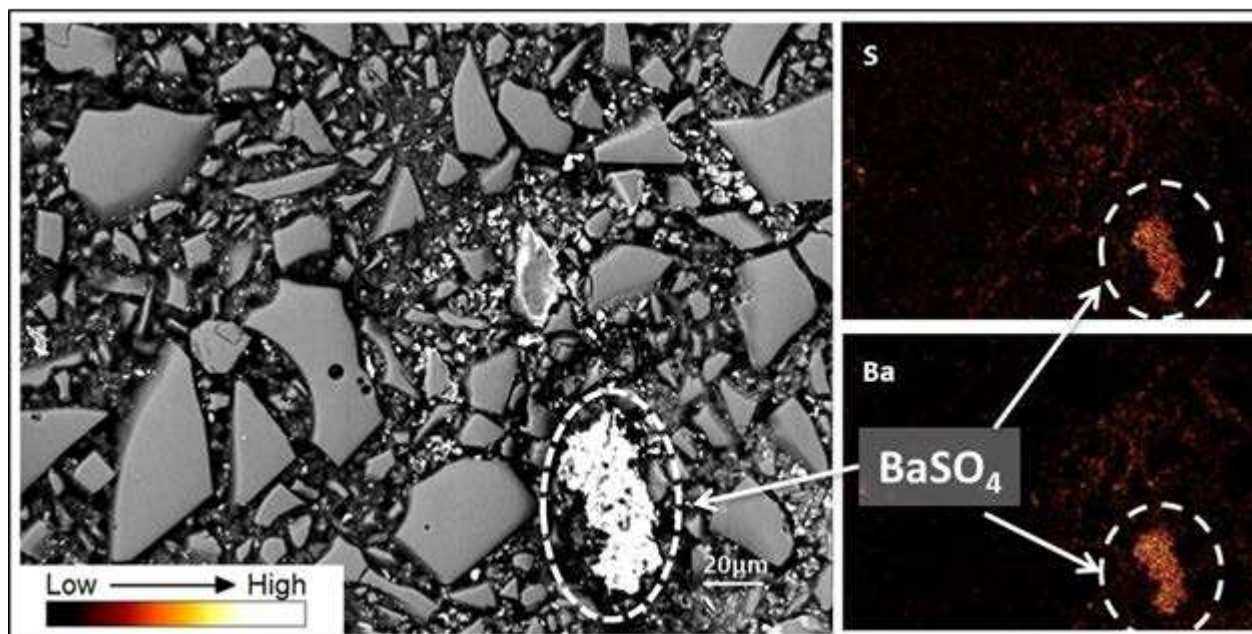
534

535 In Figure 10, there is also a small region (dashed circles in Ba and S maps) with an increased
536 concentration of Ba and S, indicating the formation of BaSO₄, with the sulphate presumably
537 made available through oxidation of the sulphide supplied by the slag. Sulphur appears to be
538 homogeneously distributed in the unreacted slag particles and also the matrix, but it is
539 particularly concentrated around the edge of what appears to be a Fe particle observed in the
540 bottom left of the micrograph (the bright white particle in the BSE image). This Fe-S rich

541 region is likely to correspond to an iron sulphide FeS_x ($1 \leq x \leq 2$), consistent with the highly
542 reducing environment in slag-rich cements [59].

543
544 Figure 11 shows a BSE image of the M1.0 sample, together with the elemental distributions
545 of sulphur and barium in the corresponding region. Angular BFS particles are dispersed
546 throughout the binding C-A-S-H phase. The formation of BaSO_4 is observed as both small
547 and larger white particles in the BSE image, confirmed by the corresponding elemental maps.
548 Some of the BaSO_4 particles appear to form particularly in the area surrounding the slag
549 particles. This indicates that Ba will react not just with the sulphur supplied by the sulphate
550 bearing solution, but also with the sulphur present in the slag, as noted above.

551



552
553 **Figure 11.** Backscattered electron image and elemental maps of sample M1.0. Ba and S
554 elemental maps confirm the formation of BaSO_4

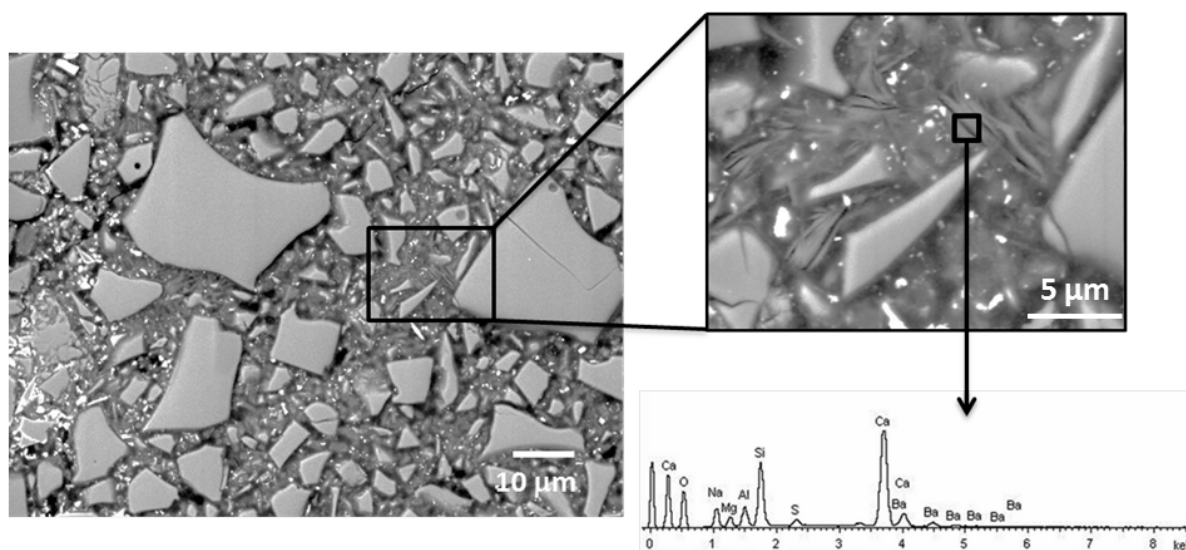
555

556

557 Figure 12 shows another region of the composite sample M1.0, where a homogeneous C-A-
558 S-H binding matrix (dark grey area), with embedded unreacted slag particles (light grey) and
559 BaSO_4 particles (white particles), is observed. The inset shows a higher magnification image
560 of a region with reduced content of BaSO_4 particles, where it is possible to identify the
561 formation of phases with microstructures comparable to the lamellar morphology observed
562 for monosulphoaluminate/ettringite compounds [60], consistent with the mineralogy
563 identified by other analytical techniques here. The EDX spectrum of this region shows the

564 incorporation of Ba in these sulphotoaluminate phases, supporting the formation of a Ba-
565 substituted ettringite as previously suggested based on XRD data.

566



567

568 **Figure 12.** Backscattered electron image of sample M1.0, with a higher-magnification view
569 of the sulphotoaluminate product formed within the gel, and an EDX spectrum of the region
570 indicated.

571

572

573 4. Conclusions

574

575 Solid composite cement binders in the system $\text{Ba}(\text{OH})_2\text{-Na}_2\text{SO}_4\text{-slag}$ can be produced via a
576 one-step method for immobilisation of sulphate bearing aqueous nuclear waste, where the
577 precipitation of BaSO_4 generates NaOH in situ to act as an activator for the slag, in addition
578 to the individual effects of the $\text{Ba}(\text{OH})_2$ and Na_2SO_4 . X-ray diffraction results confirm the
579 successful binding of sulphate in very insoluble crystalline phases such as BaSO_4 in the
580 composite samples, offering the potential for good binder stability in the long term. The
581 microstructure of the composites is dominated by the strength giving phase C-A-S-H, along
582 with layered double hydroxides (hydrotalcite and AFm type) and Ba-substituted ettringite
583 forming as secondary reaction products. Comparing the reaction products formed in the
584 composite wastefoms with those identified when activating BFS with either $\text{Ba}(\text{OH})_2$,
585 Na_2SO_4 or NaOH as a sole activator, it is seen that both Na_2SO_4 and $\text{Ba}(\text{OH})_2$ are acting as
586 alkaline activators in the composite system. An increased content of $\text{Ba}(\text{OH})_2$ in the

587 composite binders seems to favour a higher extent of reaction of the slag, and a 30% excess
588 of Ba(OH)₂ over Na₂SO₄ is seen to be sufficient to prevent the presence of free Na₂SO₄ in the
589 pore network of the binder. The inclusion of Ba also influences the chemistry of the main
590 reaction products in these composites; Ba²⁺ is able to substitute into ettringite, which reduces
591 the formation of hydrotalcite in the composite cements compared to those activated by a sole
592 activator. There also appears to be some scope for substitution of Ba²⁺ for Ca²⁺ in C-A-S-H
593 gel, particularly when no sulphate is added.

594

595

596 **Acknowledgements**

597

598 This study has been sponsored by EPSRC through the ‘Nuclear FiRST’ Doctoral Training
599 Centre at The University of Sheffield and The University of Manchester. The NMR spectra
600 were collected using the EPSRC UK National Solid-state NMR Service at Durham
601 University. The authors would like to thank Dr. Claire Utton for valuable comments and
602 discussions regarding this work, and Dr Clint Sharrad for his input into the PhD project of
603 NM.

604

605

606 **References**

- 607 [1] P.A. Bingham, R.J. Hand, Sulphate incorporation and glass formation in phosphate systems for
608 nuclear and toxic waste immobilization, *Mater. Res. Bull.*, 43 (2008) 1679-1693.
- 609 [2] R.S. Gollop, H.F.W. Taylor, Microstructural and microanalytical studies of sulfate attack. IV.
610 Reactions of a slag cement paste with sodium and magnesium sulfate solutions, *Cem. Concr. Res.*, 26
611 (1996) 1013-1028.
- 612 [3] H.F.W. Taylor, C. Famy, K.L. Scrivener, Delayed ettringite formation, *Cem. Concr. Res.*, 31
613 (2001) 683-693.
- 614 [4] F.P. Glasser, Progress in the immobilization of radioactive wastes in cement, *Cem. Concr. Res.*, 22
615 (1992) 201-216.
- 616 [5] T. Asano, T. Kawasaki, N. Higuchi, Y. Horikawa, Feasibility study of solidification for low-level
617 liquid waste generated by sulfuric acid elution treatment of spent ion exchange resin, *J Power Energy*
618 *Syst*, 2 (2008) 206-214.
- 619 [6] N. Mobasher, H. Kinoshita, S.A. Bernal, C.A. Sharrad, Ba(OH)₂ – blast furnace slag composite
620 binders for the encapsulation of sulphate bearing nuclear waste, *Advances in Applied Ceramics*,
621 (2014), in press, DOI 10.1179/1743676114Y.0000000148.
- 622 [7] D.R. Lide, *CRC Handbook of Chemistry and Physics*, 86th ed., Taylor and Francis, USA, 2005.
- 623 [8] Y. Esen, B. Yilmazer, An investigation of X-ray and radio isotope energy absorption of
624 heavyweight concretes containing barite, *Bull. Mater. Sci.*, 34 (2011) 169-175.
- 625 [9] IAEA, *Handling and Processing of Radioactive Waste for Nuclear Applications*, Technical Report,
626 Vienna, 2001.
- 627 [10] S.A. Bernal, J.L. Provis, A. Fernández-Jiménez, P.V. Krivenko, E. Kavalerova, M. Palacios, C.
628 Shi, Binder chemistry – High-calcium alkali-activated materials. In: *Alkali-Activated Materials:*

- 629 State-of-the-Art Report, RILEM TC 224-AAM, editors J.L. Provis, J.S.J. van Deventer,
630 RILEM/Springer, Dordrecht, 2014, 59-91.
- 631 [11] C. Shi, A. Fernández-Jiménez, Stabilization/solidification of hazardous and radioactive wastes
632 with alkali-activated cements, *J. Hazard. Mater.*, B137 (2006) 1656-1663.
- 633 [12] S.-D. Wang, X.-C. Pu, K.L. Scrivener, P.L. Pratt, Alkali-activated slag cement and concrete: a
634 review of properties and problems, *Adv. Cem. Res.*, 7 (1995) 93-102.
- 635 [13] I.G. Richardson, The nature of C-S-H in hardened cements, *Cem. Concr. Res.*, 29 (1999) 1131-
636 1147.
- 637 [14] A. Fernández-Jiménez, F. Puertas, I. Sobrados, J. Sanz, Structure of calcium silicate hydrates
638 formed in alkaline-activated slag: Influence of the type of alkaline activator, *J. Am. Ceram. Soc.*, 86
639 (2003) 1389-1394.
- 640 [15] I.G. Richardson, G.W. Groves, Microstructure and microanalysis of hardened cement pastes
641 involving ground granulated blast-furnace slag, *J. Mater. Sci.*, 27 (1992) 6204-6212.
- 642 [16] O. Burciaga-Díaz, J.I. Escalante-García, Structure, mechanisms of reaction, and strength of an
643 alkali-activated blast-furnace slag, *J. Am. Ceram. Soc.*, 96 (2013) 3939-3948.
- 644 [17] M. Ben Haha, B. Lothenbach, G. Le Saout, F. Winnefeld, Influence of slag chemistry on the
645 hydration of alkali-activated blast-furnace slag -- Part I: Effect of MgO, *Cem. Concr. Res.*, 41 (2011)
646 955-963.
- 647 [18] M. Ben Haha, B. Lothenbach, G. Le Saout, F. Winnefeld, Influence of slag chemistry on the
648 hydration of alkali-activated blast-furnace slag — Part II: Effect of Al₂O₃, *Cem. Concr. Res.*, 42
649 (2012) 74-83.
- 650 [19] S.A. Bernal, R. San Nicolas, R.J. Myers, R. Mejía de Gutiérrez, F. Puertas, J.S.J. van Deventer,
651 J.L. Provis, MgO content of slag controls phase evolution and structural changes induced by
652 accelerated carbonation in alkali-activated binders, *Cem. Concr. Res.*, 57 (2014) 33-43.
- 653 [20] M. Ben Haha, G. Le Saout, F. Winnefeld, B. Lothenbach, Influence of activator type on
654 hydration kinetics, hydrate assemblage and microstructural development of alkali activated blast-
655 furnace slags, *Cem. Concr. Res.*, 41 (2011) 301-310.
- 656 [21] S.D. Wang, K.L. Scrivener, Hydration products of alkali-activated slag cement, *Cem. Concr.*
657 *Res.*, 25 (1995) 561-571.
- 658 [22] P.J. Schilling, L.G. Butler, A. Roy, H.C. Eaton, ²⁹Si and ²⁷Al MAS-NMR of NaOH-activated
659 blast-furnace slag, *J. Am. Ceram. Soc.*, 77 (1994) 2363-2368.
- 660 [23] F. Bonk, J. Schneider, M.A. Cincotto, H. Panepucci, Characterization by multinuclear high-
661 resolution NMR of hydration products in activated blast-furnace slag pastes, *J. Am. Ceram. Soc.*, 86
662 (2003) 1712-1719.
- 663 [24] A. Gruskovnjak, B. Lothenbach, F. Winnefeld, R. Figi, S.C. Ko, M. Adler, U. Mäder, Hydration
664 mechanisms of super sulphated slag cement, *Cem. Concr. Res.*, 38 (2008) 983-992.
- 665 [25] Y. Bai, N.C. Collier, N.B. Milestone, C.H. Yang, The potential for using slags activated with
666 near neutral salts as immobilisation matrices for nuclear wastes containing reactive metals, *J. Nucl.*
667 *Mater.*, 413 (2011) 183-192.
- 668 [26] J. Escalante-García, A.F. Fuentes, A. Gorokhovskiy, P.E. Fraire-Luna, G. Mendoza-Suarez,
669 Hydration products and reactivity of blast-furnace slag activated by various alkalis., *J. Am. Ceram.*
670 *Soc.*, 86 (2003) 2148-2153.
- 671 [27] S.-D. Wang, K.L. Scrivener, ²⁹Si and ²⁷Al NMR study of alkali-activated slag, *Cem. Concr. Res.*,
672 33 (2003) 769-774.
- 673 [28] I.G. Richardson, A.R. Brough, R. Brydson, G.W. Groves, C.M. Dobson, Location of aluminum
674 in substituted calcium silicate hydrate (C-S-H) gels as determined by ²⁹Si and ²⁷Al NMR and EELS, *J.*
675 *Am. Ceram. Soc.*, 76 (1993) 2285-2288.
- 676 [29] F.P. Glasser, Chemistry of solidified waste forms, in: R.D. Spence (Ed.) *Chemistry and*
677 *Microstructure of Solidified Waste Forms*, Boca Raton:Lewis Publishers, US, 1993.
- 678 [30] F. Glasser, A. Kindness, S. Stronach, Stability and solubility relationships in AFm phases: Part I.
679 Chloride, sulfate and hydroxide, *Cem. Concr. Res.*, 29 (1999) 861-866.
- 680 [31] M.L.D. Gougar, B.E. Scheetz, D.M. Roy, Ettringite and C-S-H Portland cement phases for waste
681 ion immobilization: A review, *Waste Manag.*, 16 (1996) 295-303.
- 682 [32] C. Jun, C. Xin, L. Lingchao, H. Shifeng, Y. Zhengmao, High water content material based on ba-
683 bearing sulphoaluminate cement, *J. Wuhan Univ. Technol.-Mater. Sci. Ed.*, 20 (2005) 88-90.

- 684 [33] C.A. Utton, E. Gallucci, J. Hill, N.B. Milestone, Interaction between BaCO₃ and OPC/BFS
685 composite cements at 20°C and 60°C, *Cem. Concr. Res.*, 41 (2011) 236-243.
- 686 [34] D. Dermatas, X. Meng, Utilization of fly ash for stabilization/solidification of heavy metal
687 contaminated soils, *Eng. Geol.*, 70 (2003) 377-394.
- 688 [35] E. Ciliberto, S. Ioppolo, F. Manuella, Etringite and thaumasite: A chemical route for their
689 removal from cementitious artefacts, *J. Cult. Herit.*, 9 (2008) 30-37.
- 690 [36] P.M. Carmona-Quiroga, M.T. Blanco-Varela, Etringite decomposition in the presence of barium
691 carbonate, *Cem. Concr. Res.*, 52 (2013) 140-148.
- 692 [37] C. Hall, P. Barnes, A.D. Billimore, A.C. Jupe, X. Turrillas, Thermal decomposition of ettringite
693 Ca₆[Al(OH)₆]₂(SO₄)₃·26H₂O, *J. Chem. Soc. Faraday Trans.*, 92 (1996) 2125-2129.
- 694 [38] L. Alarcon-Ruiz, G. Platret, E. Massieu, A. Ehrlacher, The use of thermal analysis in assessing
695 the effect of temperature on a cement paste, *Cem. Concr. Res.*, 35 (2005) 609-613.
- 696 [39] M. Maciejewski, H.-R. Oswald, A. Reller, Thermal transformations of vaterite and calcite,
697 *Thermochim. Acta*, 234 (1994) 315-328.
- 698 [40] E. Kanazaki, Thermal behavior of the hydrotalcite-like layered structure of Mg and Al-layered
699 double hydroxides with interlayer carbonate by means of in situ powder HTXRD and DTA/TG, *Solid
700 State Ionics*, 106 (1998) 279-284.
- 701 [41] V.S. Ramachandran, C.-M. Zhang, Thermal analysis of the 3CaO·Al₂O₃-CaSO₄·2H₂O-CaCO₃-
702 H₂O system, *Thermochim. Acta*, 106 (1986) 273-282.
- 703 [42] K. Rozov, U. Berner, C. Taviot-Gueho, F. Leroux, G. Renaudin, D. Kulik, L.W. Diamond,
704 Synthesis and characterization of the LDH hydrotalcite-pyroaurite solid-solution series, *Cem. Concr.
705 Res.*, 40 (2010) 1248-1254.
- 706 [43] S.A. Bernal, J.L. Provis, B. Walkley, R. San Nicolas, J.D. Gehman, D.G. Brice, A.R. Kilcullen,
707 P. Duxson, J.S.J. van Deventer, Gel nanostructure in alkali-activated binders based on slag and fly
708 ash, and effects of accelerated carbonation, *Cem. Concr. Res.*, 53 (2013) 127-144.
- 709 [44] G. Engelhardt, D. Michel, High-Resolution Solid-State NMR of Silicates and Zeolites, John
710 Wiley & Sons, Chichester, 1987.
- 711 [45] J.R. Barnes, A.D.H. Clague, N.J. Clayden, C.M. Dobson, C.J. Hayes, G.W. Groves, S.A. Rodger,
712 Hydration of Portland cement followed ²⁹Si solid-state NMR spectroscopy, *J. Mater. Sci. Lett.*, 4
713 (1985) 1293-1295.
- 714 [46] G. Le Saoût, M. Ben Haha, F. Winnefeld, B. Lothenbach, Hydration degree of alkali-activated
715 slags: A ²⁹Si NMR study, *J. Am. Ceram. Soc.*, 94 (2011) 4541-4547.
- 716 [47] M.D. Andersen, H.J. Jakobsen, J. Skibsted, Incorporation of aluminum in the calcium silicate
717 hydrate (C-S-H) of hydrated Portland cements: A high-field ²⁷Al and ²⁹Si MAS NMR investigation,
718 *Inorg. Chem.*, 42 (2003) 2280-2287.
- 719 [48] R.J. Myers, S.A. Bernal, R. San Nicolas, J.L. Provis, Generalized structural description of
720 calcium-sodium aluminosilicate hydrate gels: the cross-linked substituted tobermorite model,
721 *Langmuir*, 17 (2013) 5294-5306.
- 722 [49] M.D. Andersen, H.J. Jakobsen, J. Skibsted, A new aluminium-hydrate species in hydrated
723 Portland cements characterized by ²⁷Al and ²⁹Si MAS NMR spectroscopy, *Cem. Concr. Res.*, 36
724 (2006) 3-17.
- 725 [50] S. Kwan, J. LaRosa, M.W. Grutzeck, ²⁹Si and ²⁷Al MASNMR study of strätlingite, *J. Am.
726 Ceram. Soc.*, 78 (1995) 1921-1926.
- 727 [51] J.M. Rivas Mercury, P. Pena, A.H. De Aza, X. Turrillas, I. Sobrados, J. Sanz, Solid-state ²⁷Al
728 and ²⁹Si NMR investigations on Si-substituted hydrogarnets, *Acta Mater.*, 55 (2007) 1183-1191.
- 729 [52] H. Koller, G. Engelhardt, A.P.M. Kentgens, J. Sauer, ²³Na NMR spectroscopy of solids:
730 Interpretation of quadrupole interaction parameters and chemical shifts, *J. Phys. Chem.*, 98 (1994)
731 1544-1551.
- 732 [53] C. Shi, P.V. Krivenko, D.M. Roy, *Alkali-Activated Cements and Concretes*, Taylor & Francis,
733 Abingdon, UK, 2006.
- 734 [54] C. Shi, On the state and role of alkalis during the activation of alkali-activated slag cement, in:
735 *Proceedings of the 11th International Congress on the Chemistry of Cement*, Durban, South Africa,
736 2003.

- 737 [55] T.T.H. Bach, E. Chabas, I. Pochard, C. Cau Dit Coumes, J. Haas, F. Frizon, A. Nonat, Retention
738 of alkali ions by hydrated low-pH cements: Mechanism and Na⁺/K⁺ selectivity, *Cem. Concr. Res.*, 51
739 (2013) 14-21.
- 740 [56] F. Puertas, A. Fernández-Jiménez, M.T. Blanco-Varela, Pore solution in alkali-activated slag
741 cement pastes. Relation to the composition and structure of calcium silicate hydrate, *Cem. Concr.*
742 *Res.*, 34 (2004) 139-148.
- 743 [57] S.A. Bernal, J.L. Provis, V. Rose, R. Mejía de Gutiérrez, High-resolution X-ray diffraction and
744 fluorescence microscopy characterization of alkali-activated slag-metakaolin binders, *J. Am. Ceram.*
745 *Soc.*, 96 (2013) 1951-1957.
- 746 [58] J. Skibsted, M.D. Andersen, The effect of alkali ions on the incorporation of aluminum in the
747 calcium silicate hydrate (C-S-H) phase resulting from Portland cement hydration studied by ²⁹Si
748 MAS NMR, *J. Am. Ceram. Soc.*, 96 (2012) 651-656.
- 749 [59] M. Atkins, F.P. Glasser, Application of Portland cement-based materials to radioactive waste
750 immobilization, *Waste Manag.*, 12 (1992) 105-131.
- 751 [60] K.L. Scrivener, Backscattered electron imaging of cementitious microstructures: understanding
752 and quantification, *Cem. Concr. Compos.*, 26 (2004) 935-945.

753